MECHANICAL ENGINEERING DEPARTMENT

[redacted]

SCHOOL OF ENGINEERING
THE UNIVERSITY OF CONNECTICUT
STORRS, CONNECTICUT

ELEVATED TEMPERATURE BIAXIAL FATIGUE
Semi-Annual Status Report
Grant No. NAG-3-160
August 15, 1983 - February 15, 1984

Submitted to:

Lewis Research Center
National Aeronautics and Space Administration
21000 Brookpark Road
Clevelnd, Ohio 44135

Principal Investigator:

Eric H. Jordan
Associate Professor
Department of Mechanical Engineering
University of Connecticut
Storrs, CT 06268

INTRODUCTION

The research program described in the report deals with elevated temperature biaxial fatigue. This program is in its third year which ends February 15, 1984.

Biaxial fatigue is often encountered in the complex thermo-mechanical loadings present in gas turbine engines. Engine strain histories can involve non-constant temperature, mean stress, creep, environmental effects, both isotropic and anisotropic materials and non-proportional loading. Life prediction for the general case involving all the above factors is not tractable research project. The current research program is limited to isothermal fatigue at room temperature and 1200°F of Hastalloy-X for both proportional and non-proportional loading.

The goal of the project is to develop improved method for predicting the fatigue life and deformation response under biaxial cyclic loading. This goal will be achieved by emphasising two facets of the program. First, the experimental set-up will incorporate several unique features that are expected to give improved data quality. These features will be described in detail later in the report. Second, the relative role of elastic and plastic strain will be experimentally studied in a unique experimental program involving inert atmosphere testing.

The advancements in multiaxial fatigue to date have been made with little consideration to the question of whether multiaxial fatigue parameters should be based on total strain, plastic strain, elastic strain, or a combination of these three. The choice is not terribly important for isothermal constant rate tests involving proportional loading where these three strains tend to vary concurrently. However, under conditions often encountered in gas turbine engines involving either non-proportional loading, variable strain rate, variable temperature conditions or combinations of these, the three components of strain will not vary monotonically with one another and the identification of the correct strain components becomes all important.

The advantage of devloping a life prediction approach based on the correct identification of the damaging component of strain is that the near infinite variety of different types of non-proportional loading cycles could be handled if a reasonably valid constitute question were available. It is hoped that in addition, the effect of temperature and anisotropy may be accounted for at least in part by understanding their effect on flow behavior.

Progress made to date consists of design and construction work on the experimental facility including creation of a new laboratory area for carrying out the program. A tension torsion servo hydraulic machine has been

built using a University of Connecticut design load frame and commercially available actuators and electronics.

More economical thinner grips and the optimum gage length were determined. The operating functions of capacitive probes in elevated temperature were comfirmed to be consistent with that of room temperature. Some computer programs were modified or developed recently. The vacuum chamber had been delivered. Some features of extensometer were modified and improved. Using the outer and inner ring probes, one cycle of biaxial loading had been run. Several elevated temperature fatigue tests (in phase) and one non-proportional loading test were run satisfactorily.

The Grips

The grip currently being used is a disposable grip made of 304 stainless steel that will be pressed on and welded. The thickness of welded grips had been reduced from 1" to 3/4" and worked successfully for room and elevated temperature fatigue tests. The 3/4" grips will be cheaper than the previous 1" thick grips.

The Elevated Temperature Fatigue Tests

For elevated temperature fatigue tests, the failure of the specimen sometimes occurred at the extensometer attachment under the testing condition of 1" gage length.

The gage length was increased to move the extensometer attachment to the specimen transitions where the wall thickness is slightly greater.

Through several unsuccessful tests at various gage lengths it was determined that a gage length of 1.3 inches put the attachment sufficiently far up the transition to prevent all attachment failures. If the strain were perfectly uniform increasing the gage length from 1 to 1.3 inches should have increased the displacement at a given strain by 30%. In actual fact the strain increase was 1.5% less indicating that even at 1.3 inches the gage length has fairly uniform strain. The uniformity of strain is due to the extremely gradual transition of the OD actually being only 0.0225 inches larger at 1.3 inches than in the center of the gage length. The calibration of the 1.3 in gage length was done using a strain gage rosette.

Whether the calibration factor of the capacitance probes changes with temperature is important. By using the RVDT and a special small stroke DCDT it was possible to do a calibration of room temperature relative to elevated temperature. The extensometer was mounted on a specimen that had been cut in half. The result was that the calibration factor did not measurablely change at elevated temperature.

Computer Programs

The software system for running tests and data reduction has been modified and well developed. The computer programs are introduced briefly as follows:

INTACT: Input all the informations which are needed to run a fatigue test.

TEST: Input the desired strain rate and run the fatigue test.

PROC: From the stored data, compute the stresses, strains, such as maximum shear strain, octahedral shear strain ... etc.

PLAS: Compute the applied strain ratio, applied strain/stress range, and cyclic plastic work.

IN: Input and create the data files for general plotting.

PLOT: Does the general plotting in the X-Y plotter.

PLOT 1: Plotting: the shear strain range and normal strain range versus the angle of plane (0° - 90°).

PLOT 2: Plotting: the axial strain vs. torsional strain for checking the "phase shift angle".

PLOT 3: Plotting: (1) applied axial stress vs. axial strain. (2) applied shear stress vs. torsional strain for a selected cycle.

RTEST: A modified TEST program for checking the behaviors of ring probes, only for single cycle tests.

The Vacuum Chamber

The vacuum chamber had been ordered and recently delivered. One part was sent back to the vendor for repair of a defect. The vacuum system is expected to be set-up completely as soon as all the parts are delivered.

The Extensometer:

Some features of extensometer were modified or developed to work better. The redesigned mounting brackets of outer and inner ring probe were made and worked well. New torsional targets were made of two seperate pieces which will assure the targets remain square with the extensometer, shown in Fig. 1. New PWA 1480 supporting tips of extensometer was used and worked well.

Outer Ring Probe

The outer ring probe is a recently developed capacitance displacement probe which is 2" O.D., 1.3" I.D. and .125" thick. One calibration gage Fig. 2 with three different diameter was used to check the performance of the outer ring probe. The outer ring probe will measure the specimen O.D. change. It was found to have edge effect 1" from a free end and transition influence .45" from a step of diameter change.

The effect of the concentricity of the ring probe with the part being measured was investigated. The results of the investigation are illustrated in Fig. 3-4. From the investigation the conclusions drawn are as follows:

1. The output voltages of outer ring probe is maximum when the ring probe is set concentrially with the specimen, shown as Fig. 3.

2. For the .7" O.D. specimen and the existing outer ring probe, the allowable eccentricity is .005" which will cause 1.5% error of ring probe output, shown as Fig. 4.

3. The error of ring probe output due to the eccentricity is dependent on the distance between the specimen and ring probe. For a same eccentricity, the smaller distance between the specimen and ring probe, the smaller the error is.

Inner Ring Probe

The inner ring probe is also a capacitance displacement probe which sensor disc is .375" diameter and .05" thick. The inner ring probe has the same performing function as the outer ring probe. Since the inner ring probe will measure the specimen I.D. change, a gage shown in Fig. 5 which was made of three different I.D. (.495", .500", .505") drill bushings had been used for calibration. Similar to the properties of outer ring probe, to mount the inner ring probe, it was move around inside the specimen until the probe output reach the maximum value.

Test Results

The testing conditions and results are shown in Table 1. This data has been plotted according to a number of popular multiaxial fatigue theories including plastic work theory, modified plastic work theory, octahedral total strain theory, maximum shear strain theory, maximum plastic shear strain theory, maximum normal strain theory, and gama plane theory shown in Fig. 6-12. Each single parameter theory was least square fit as a straight line in log-log space. These linear regressions yielded

correlation coefficients that are a measure of the success of the various theories. In table 2 and 3 the correlation coefficients are reported and the theories are listed starting with the most successful and progressing to less successful theories. From these tables plastic work theory appear the most successful. Some typical plots of shear strain range and normal strain range vs. angle of planes (0° - 90°) are shown in Fig. 13-20.

In looking at these plots, it is worth pointing out that the 1200°F tests at $\lambda = 1.5$ involved unintentional non-proportional loading due to a phase lag in one controller. This data is therefore somewhat suspect. Several additional points are worth noting. First in the room temperature tests the cracks are all on the maximum shear strain planes as reported by Kanazawa et .al. (ref. 1) but at 1200°F all cracking is on maximum normal strain planes. The direction of cracking at 1200°F is suggestive of a mechanism change and also suggests that the theory of Brown and Miller may not be applicable. It is also worth noting that unlike the data in the paper by Jordan et .al. (ref. 2) plastic work theory does not predict the non-proportional loading results well.

Summary

The major progress achieved in this reporting period was to make fully operational the 1200°F testing capability. This involved dealing with failure induced by the extensometer attachment that was not present in the room temperature testing. It was also necessary to add an interior heater to achieve acceptable temperature distributions. A significant number of computer programs were written for data reduction and control. The performance of the ring probes was investigated. It was found that they are sensitive to concentricity and exhibit sensitivity to diameters over a distance of an inch or so. The concentricity behavior requires that concentricity be maintained to approximately 0.005 inches. The sensitivity of the outer ring probe is disappointedly low and it may be of marginally usefulness. The inner ring probe appear to be satisfactory. It appears that ring probes require smaller gaps than we currently have on the outer ring probe to be successful.

Now that the high temperature capability is established rapid growth in the data base is expected in the next reporting period. The most successful theory is plastic work theory to date. However, no theory correlates the data within scatter and finding or developing one that does is the goal and challenge for the remainder of the project.

Notation: (for Table 1)

$\Delta\varepsilon$ = applied axial strain range

$\Delta\gamma$ = applied torsion strain range

λ = applied strains ratio

ϕ = phase angle

N_f = fatigue life

ΔS = applied normal stress range

$\Delta\tau$ = applied shear stress range

$\Delta\varepsilon p$ = applied platic axial strain range

$\Delta\gamma p$ = applied plastic torsional strain range

$\Delta Wp,\varepsilon$ = axial platic work

$\Delta Wp,\gamma$ = torsional plastic work

ΔWp = total plastic work

$\Delta\gamma_{oct}$ = Octahedral shear strain range

$\Delta\gamma_{max}$ = maximum shear strain range

$\Delta\varepsilon N$ = normal strains range (i.e. $\Delta\varepsilon x$) on the plane of maximum shear strains

$\Delta\sigma N$ = normal stress range (i.e. $\Delta\sigma x$) on the plane of maximum shear strains

ψ_{max} = angle of the plane of maximum shear strain (ccw from the axial direction)

$\Delta\gamma_{map},p$ = maximum plastic shear strain range

TABLE 1

Spec. No.	14	16	17	18	19	20
Temp. °F	RT	1200	1200	1200	1200	1200
λ	4	1.5	1.5	∞	∞	1.5
ϕ	0	0	0	0	0	90°
N_f, cycles	22,124	2,625	11,860	15,920	3,000	5,750
$\Delta\varepsilon$, %	.4085	.646	.395	0	0	.512
$\Delta\gamma$, %	1.567	.957	.563	1.165	2.059	.752
ΔS, psi	62,429	98,796	77,969	0	0	104,298
$\Delta\tau$, psi	69,708	44,985	34,882	63,434	78,068	57,085
$\Delta\varepsilon p$, %	.1701	.2377	.0748	0	0	.0886
$\Delta\gamma p$, %	.8879	.3914	.1928	.4212	1.111	.0893
ΔWp, ε(psi)	70	188	46	0	0	67
ΔWp, γ(psi)	423	132	32	201	703	36
ΔWp (psi)	493	320	78	201	703	103
$\Delta\gamma_{oct}$, %	1.387	1.158	.696	.9514	1.682	.6992
$\Delta\gamma_{max}$, %	1.667	1.316	.789	1.165	2.059	.7667
$\Delta\gamma_{max,p}$ %	1.028	.5665	.2032	.4565	1.193	.1169
$\Delta\varepsilon N$, %	.1234	.1943	.1284	0	0	.5138
$\Delta\sigma N$, psi	22,241	50,316	40,804	2,186	2,672	29,529
ψ_{max}, degree	80	22	22	0	0	9

TABLE 2

Theories	Correlation Coefficient RT
ΔWp	- .9561
ΔWp^*	- .9448
$\Delta\varepsilon 1$	- .9326
$\Delta\gamma_{oct}$	- .8989
$\Delta\gamma_{max}$	- .8129
$\Delta\gamma_{max,p}$	- .7850

TABLE 3

Theories	Correlation Coefficient 1200°F
ΔWp^*	- .9248
ΔWp	- .8703
$\Delta\gamma_{oct}$	- .8517
$\Delta\gamma_{max,p}$	- .8328
$\Delta\gamma_{max}$	- .8132
$\Delta\varepsilon 1$	- .7818

Note: ΔWp^*: modified cyclic plastic work

$\Delta\varepsilon 1$: maximum normal strain range

Notes

1. Young's modulus at RT, E=28.0E+6 psi
   at 1200°F, E=22.65E+6 psi

2. Shear modulus at RT, G=11.51E+6 psi
   at 1200°F, G=8.84E+6 psi

3. Poisson's ratio used to compute $\Delta\gamma_{oct}$, $\Delta\gamma_{max}$, $\Delta\gamma_{max.p}$, $\Delta\varepsilon n$, ψ_{max} are .4.

REFERENCES

1. K. Kanazawa, K. J. Miller, and M. W. Brown, "Low-Cycle Fatigue Under Out-of-Phase Loading conditions", July 1977, Transactions of the ASME.

2. Jordan, E. H., Brown, M. W., and Miller, K. J., "Fatigue Under Sever Non-proportional Loading". To appear for International Symposium on Biaxial/Multiaxial Fatigue and ASTM Symposium, December 15-17, 1982, San Francisco.

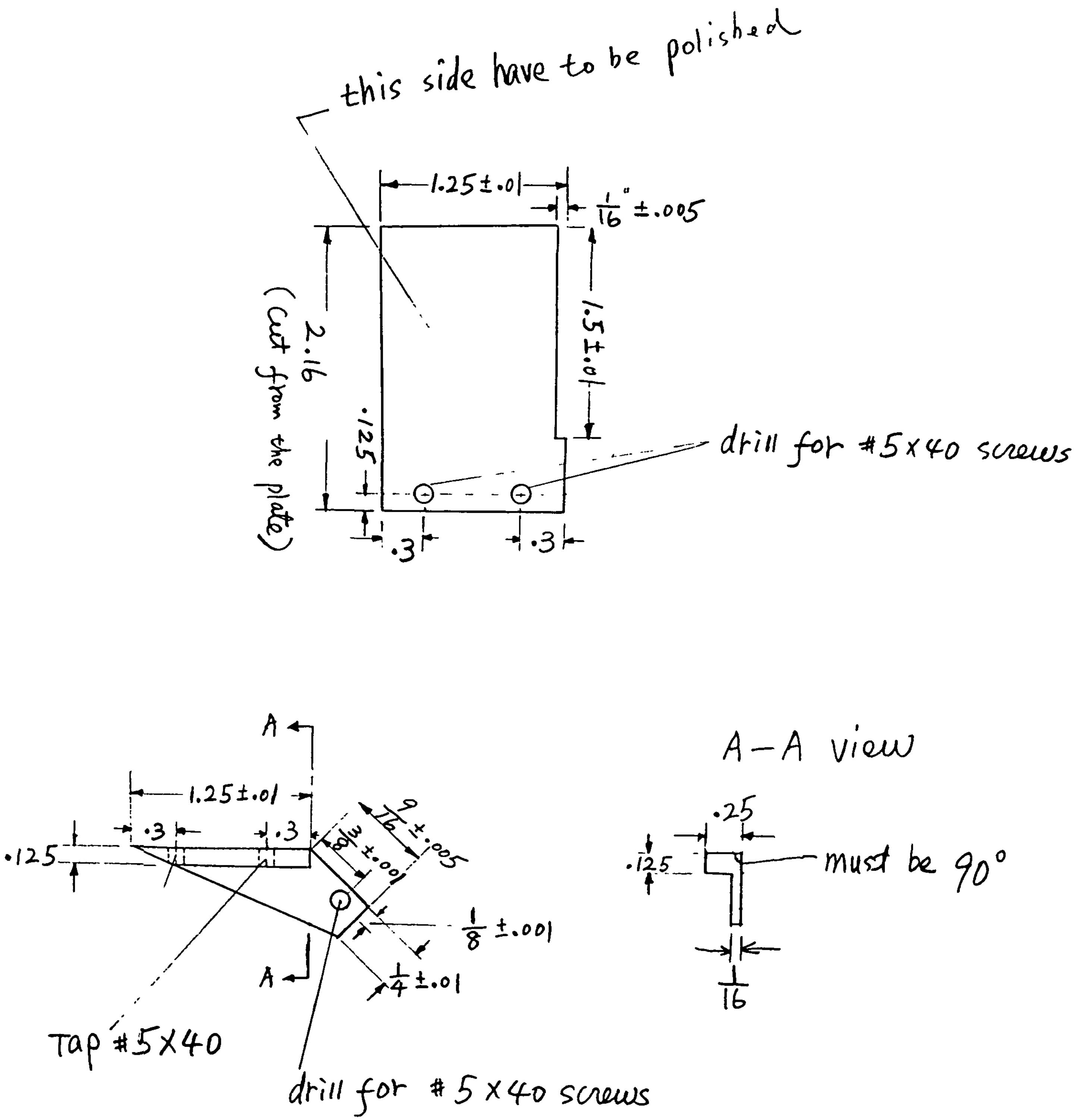

Torsional target (made of Hastelloy-X)

Fig. 1

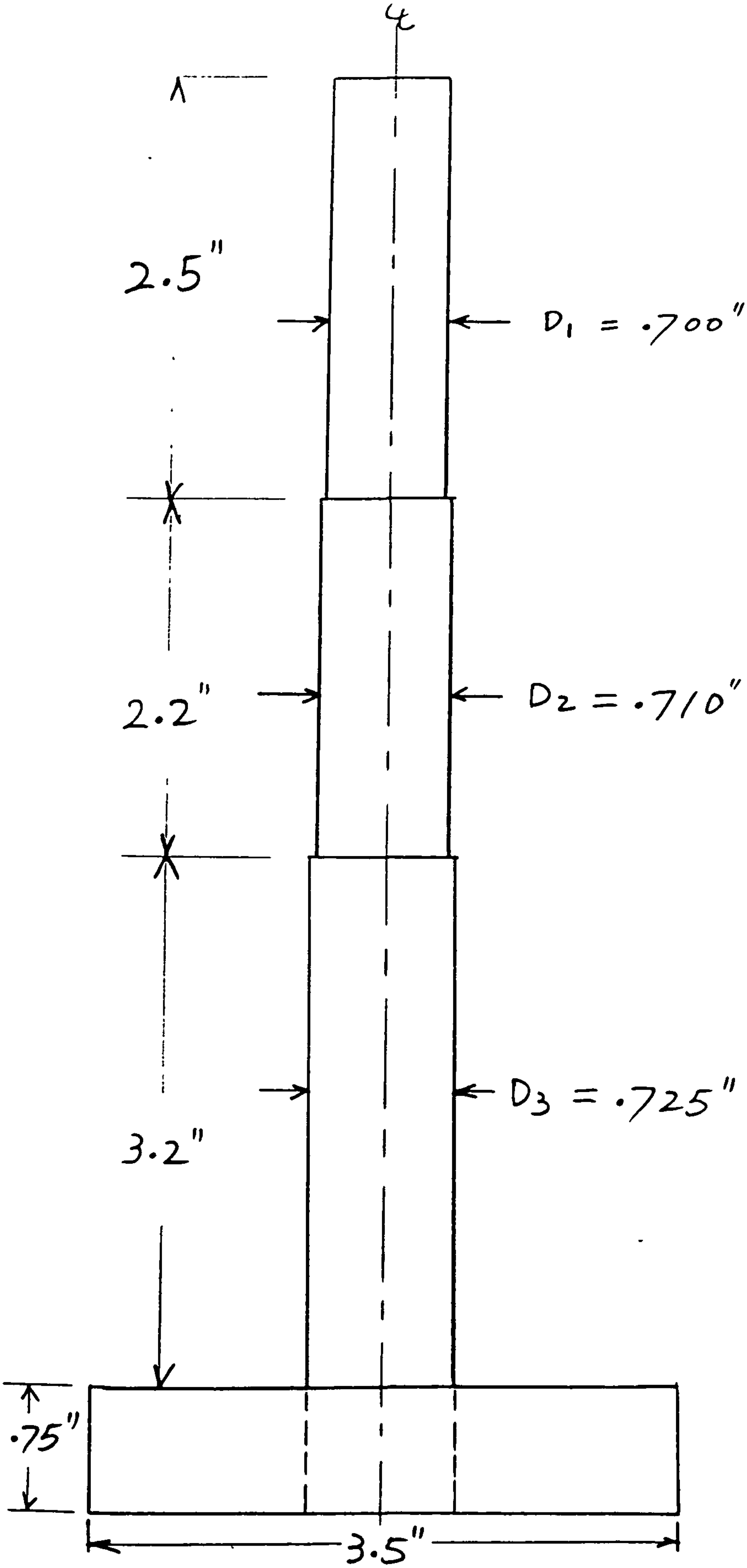

Fig. 2

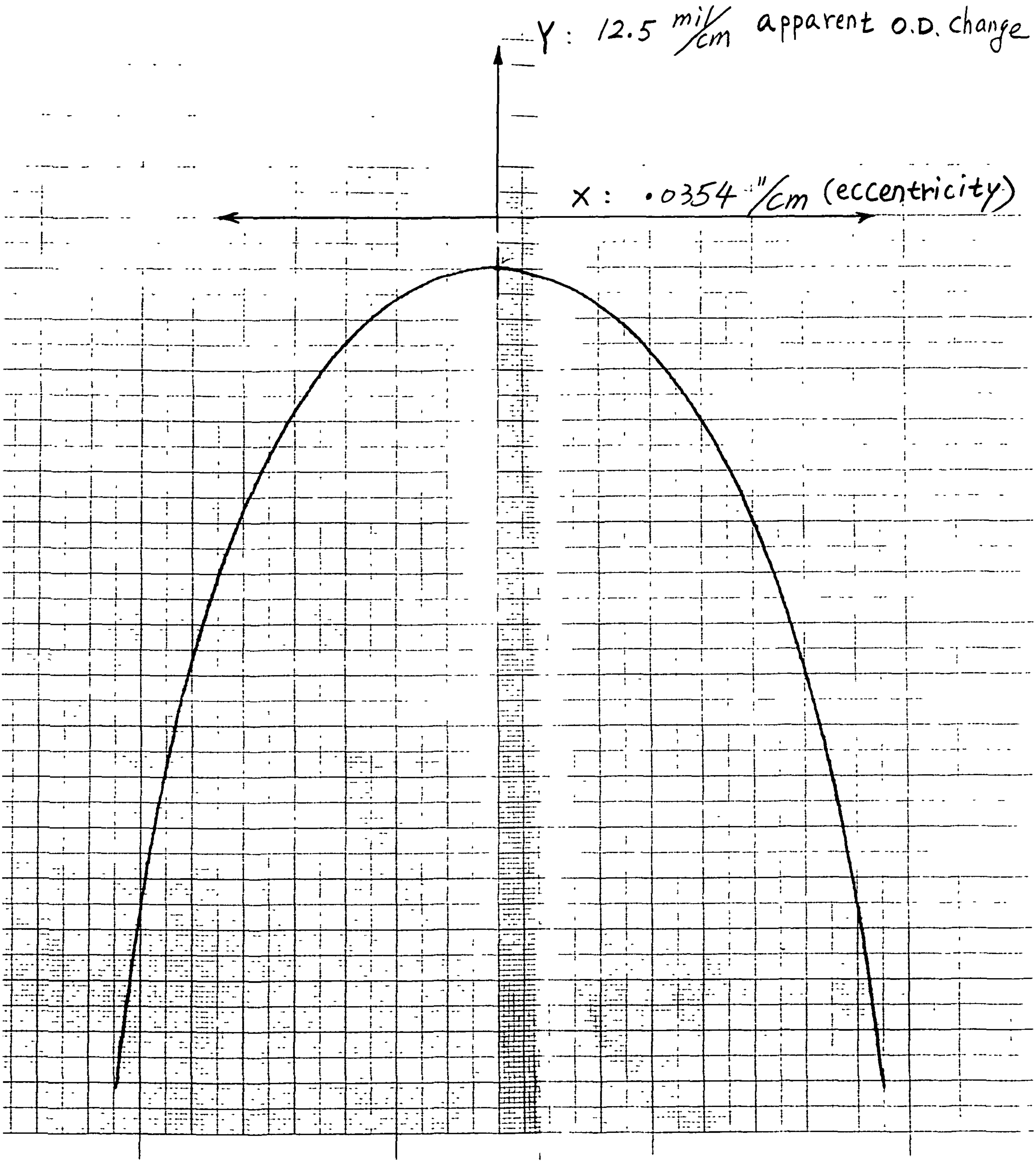

Fig. 3

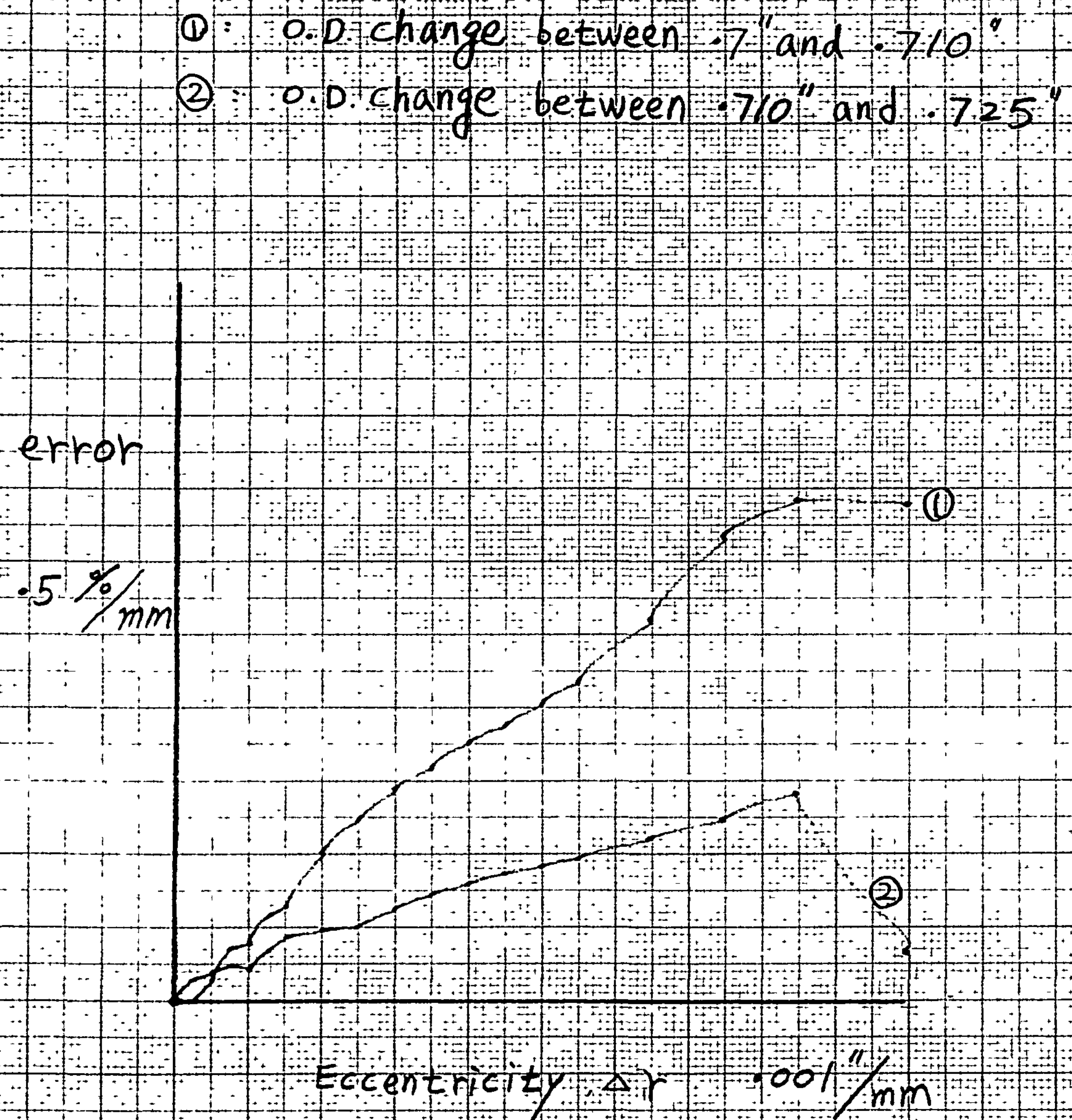
①: O.D change between .7" and .710"
②: O.D. change between .710" and .725"
error
.5 %/mm
①
②
Eccentricity Δr .001"/mm

Fig. 4

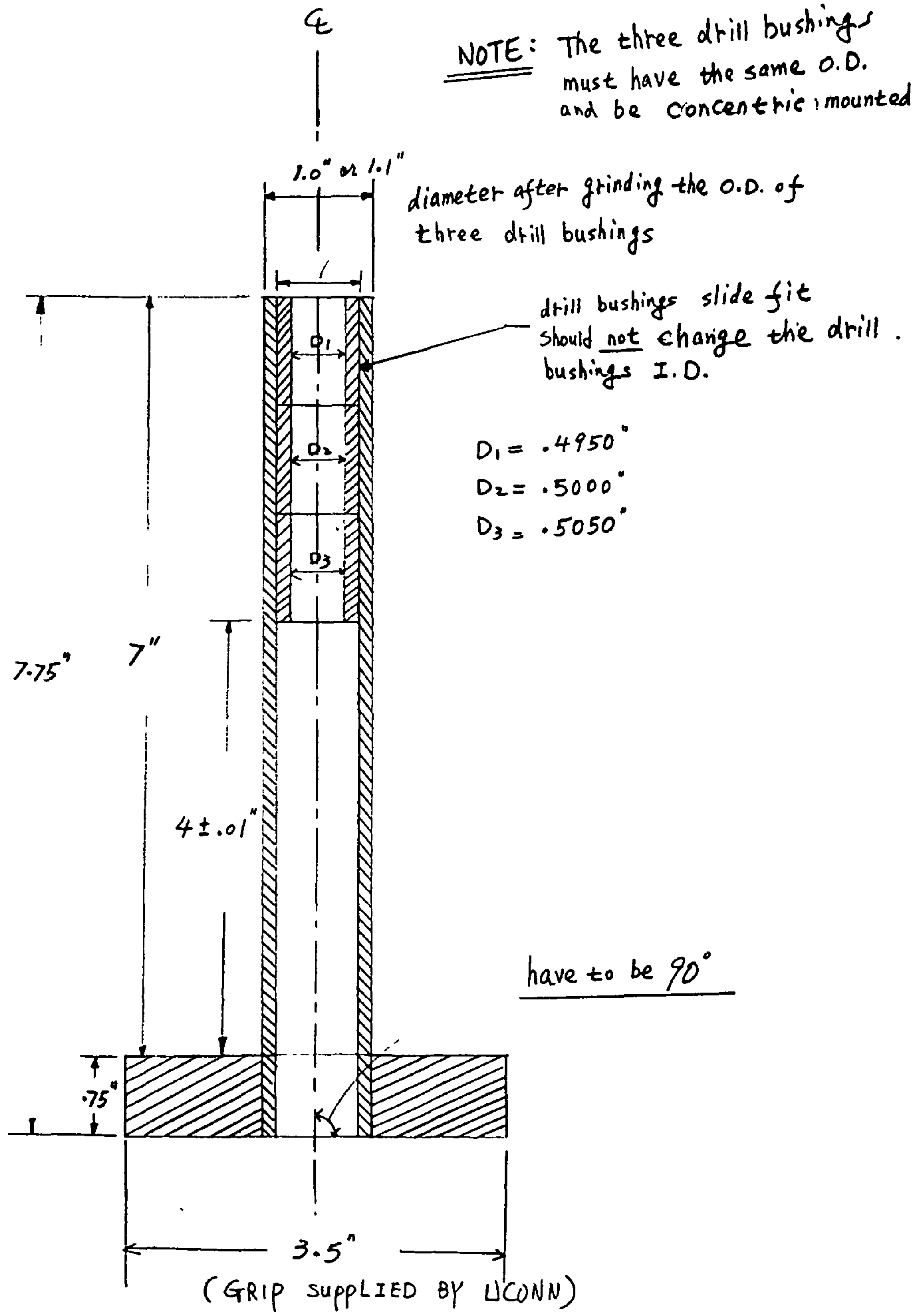

NOTE: The three drill bushings must have the same O.D. and be concentric mounted
1.0" or 1.1"
diameter after grinding the O.D. of three drill bushings
drill bushings slide fit Should not change the drill bushings I.D.
D1
D2
D3
D1 = .4950"
D2 = .5000"
D3 = .5050"
7.75"
7"
4±.01"
have to be 90°
.75"
3.5"
(GRIP SUPPLIED BY UCONN)

Fig. 5

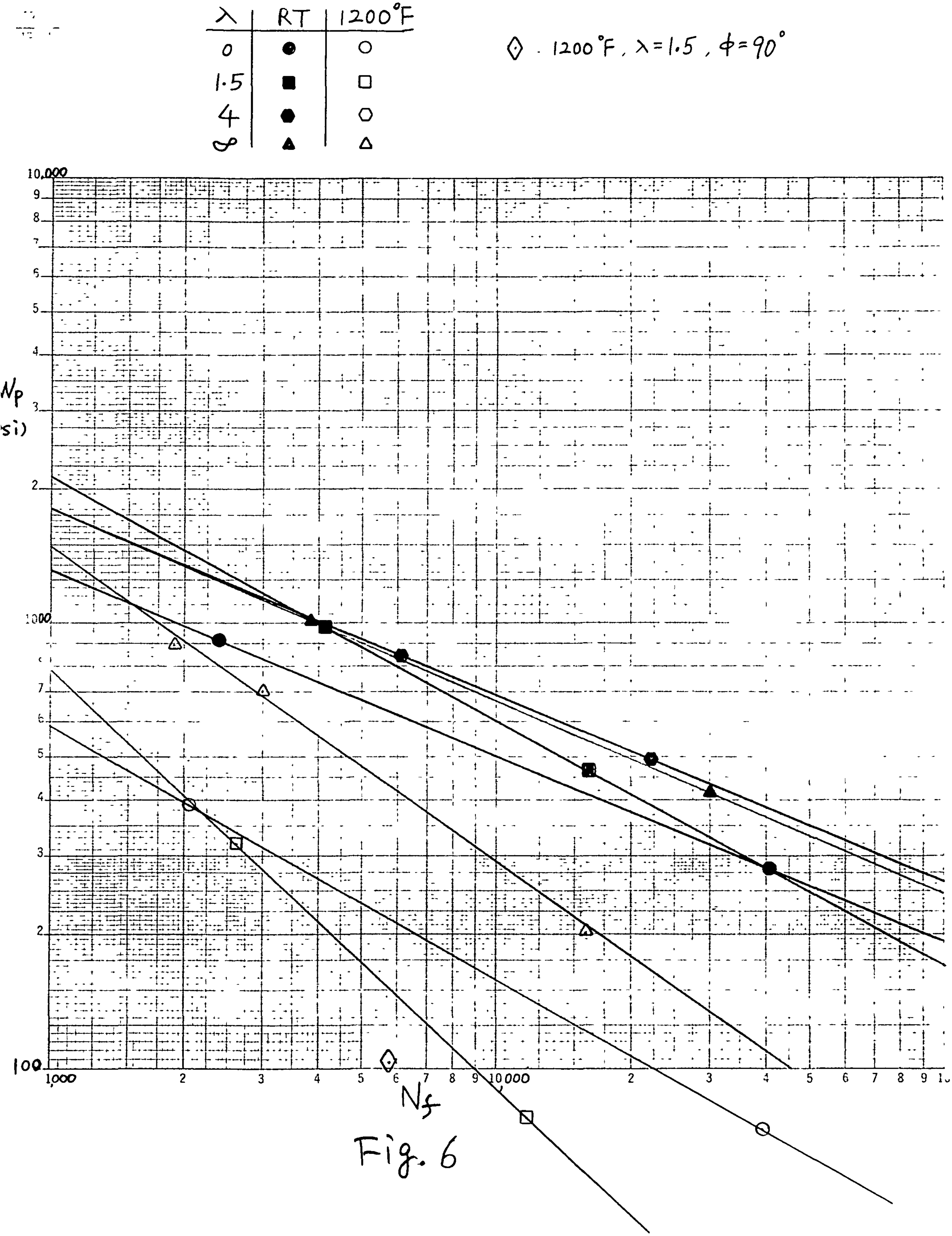

Fig. 6

Logarithmic, 2 x 2 Cycles

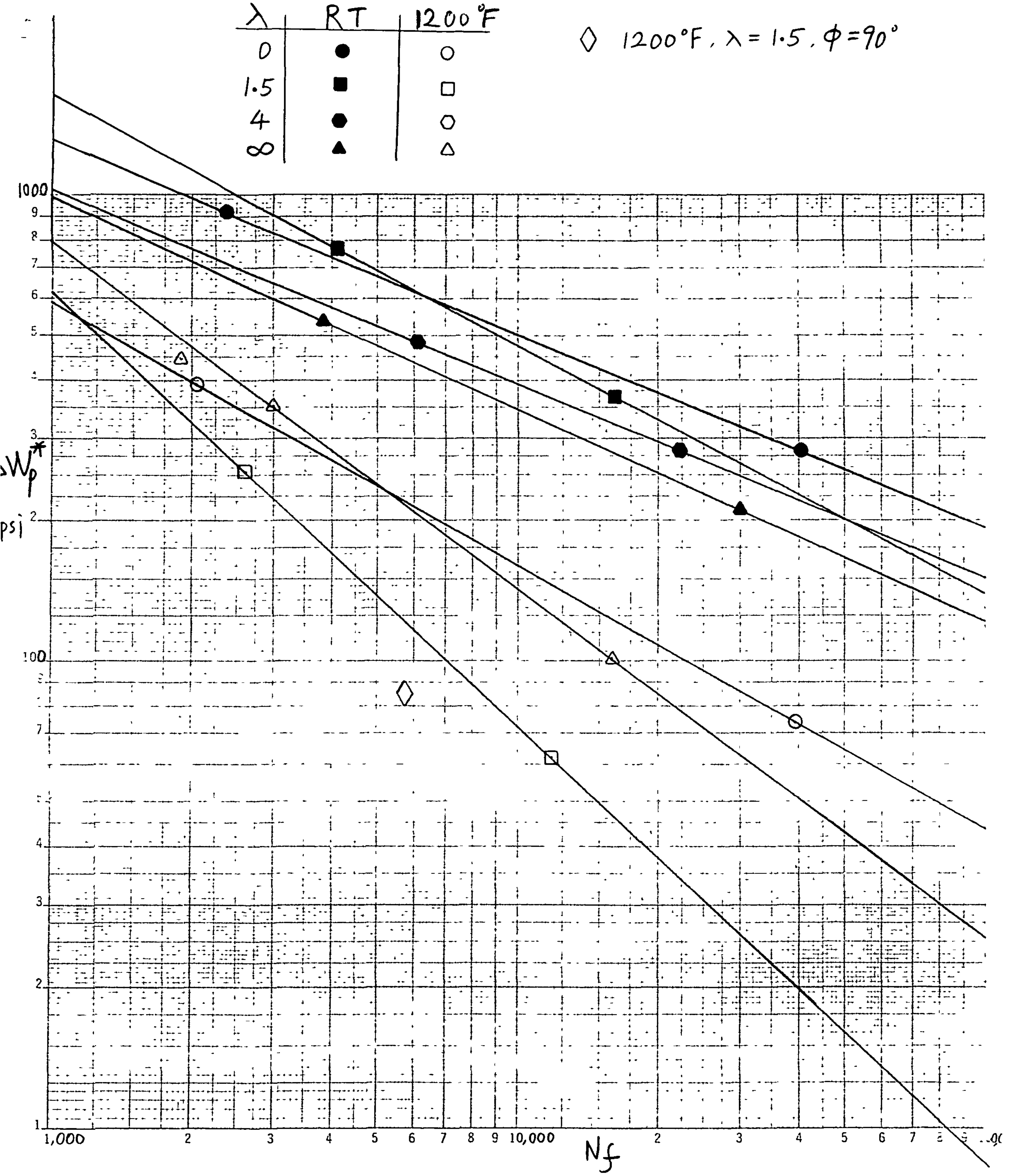

Fig. 7

Logarithmic 3 X 2 Cycles

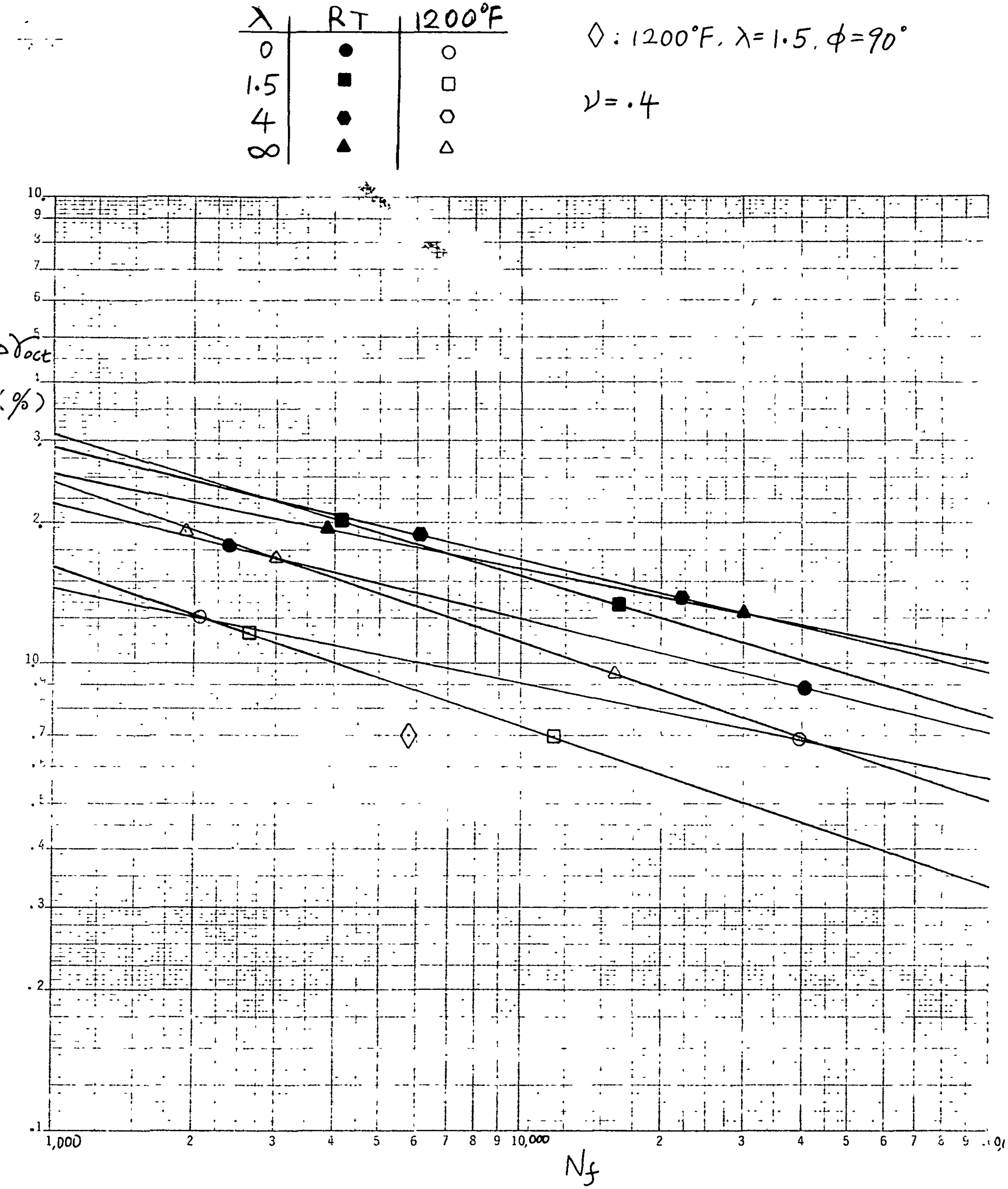

Fig. 8

Logarithmic, 2 x 2 Cycles

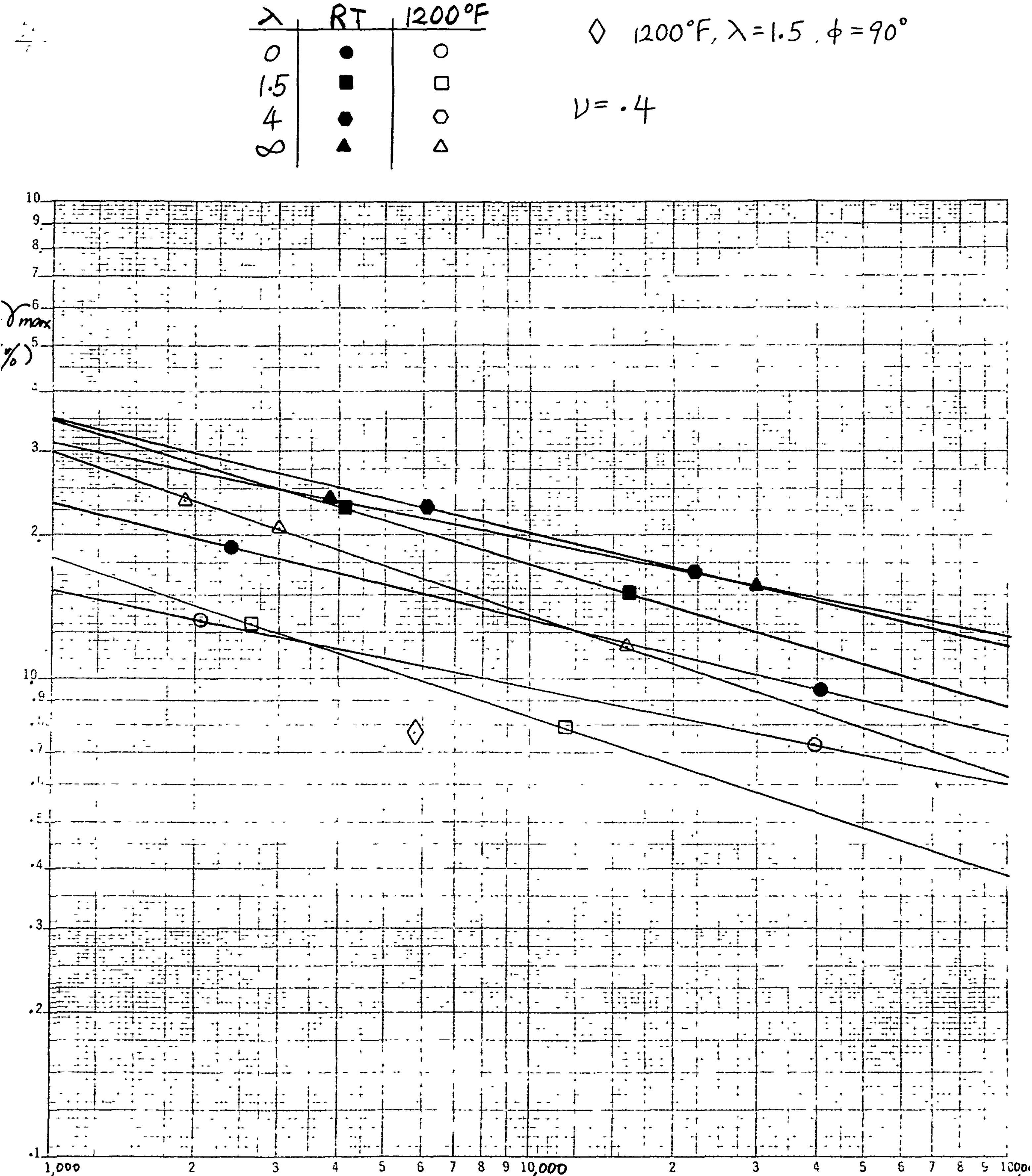

Fig. 9

Logarithmic, 2 x 2 Cycles

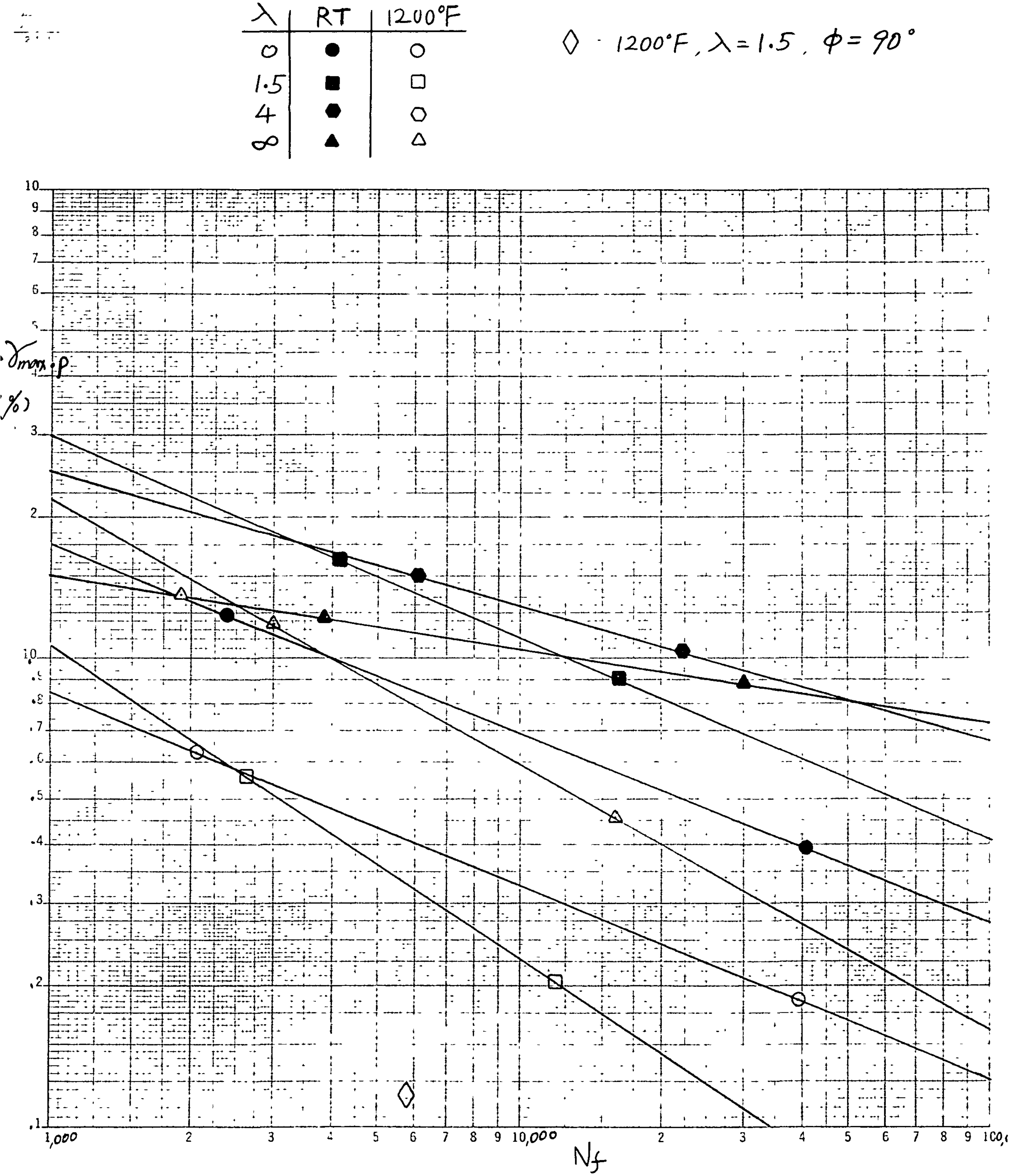

Fig. 10

Logarithmic, 2 x 3 Cycles

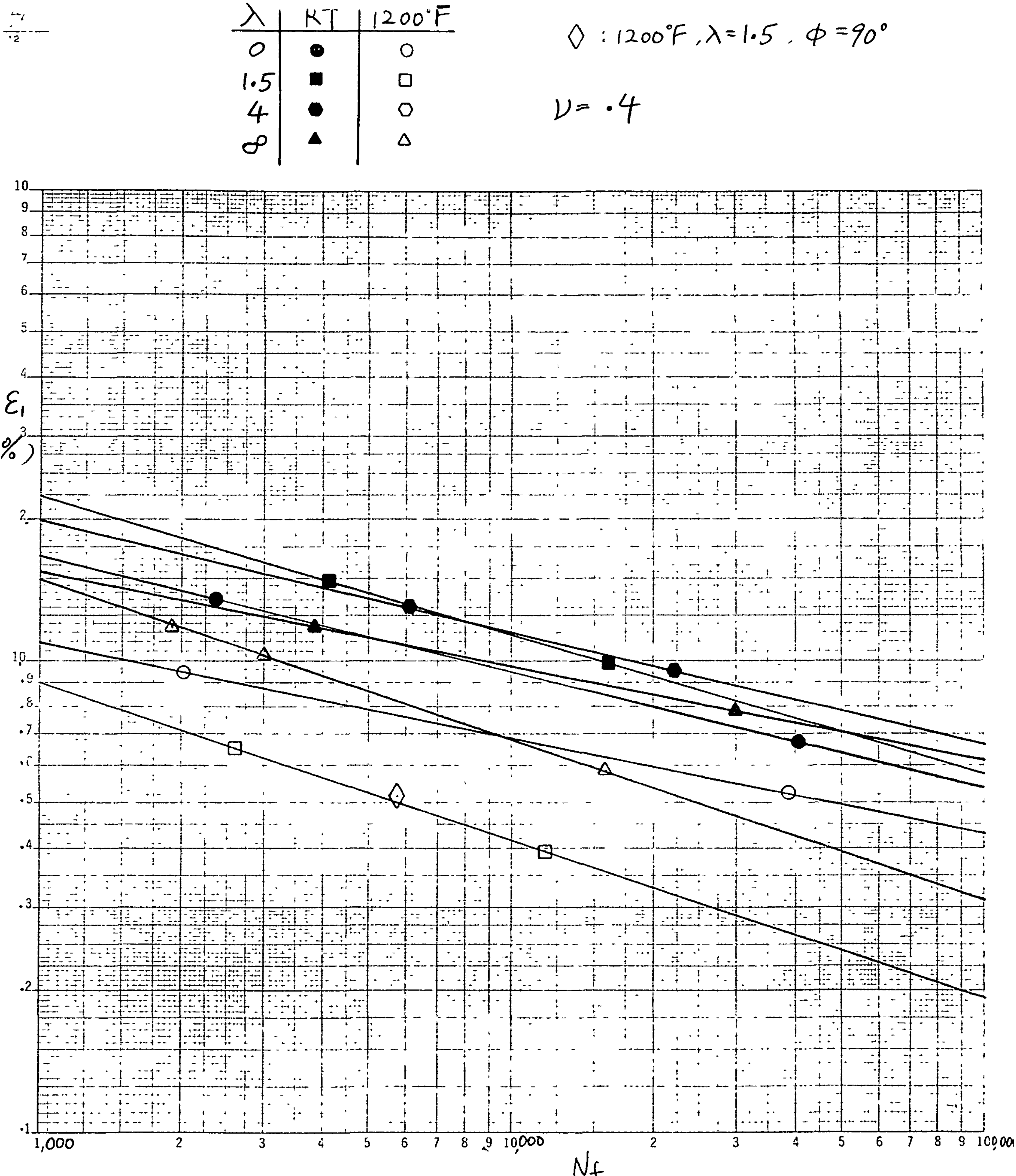

Fig. 11

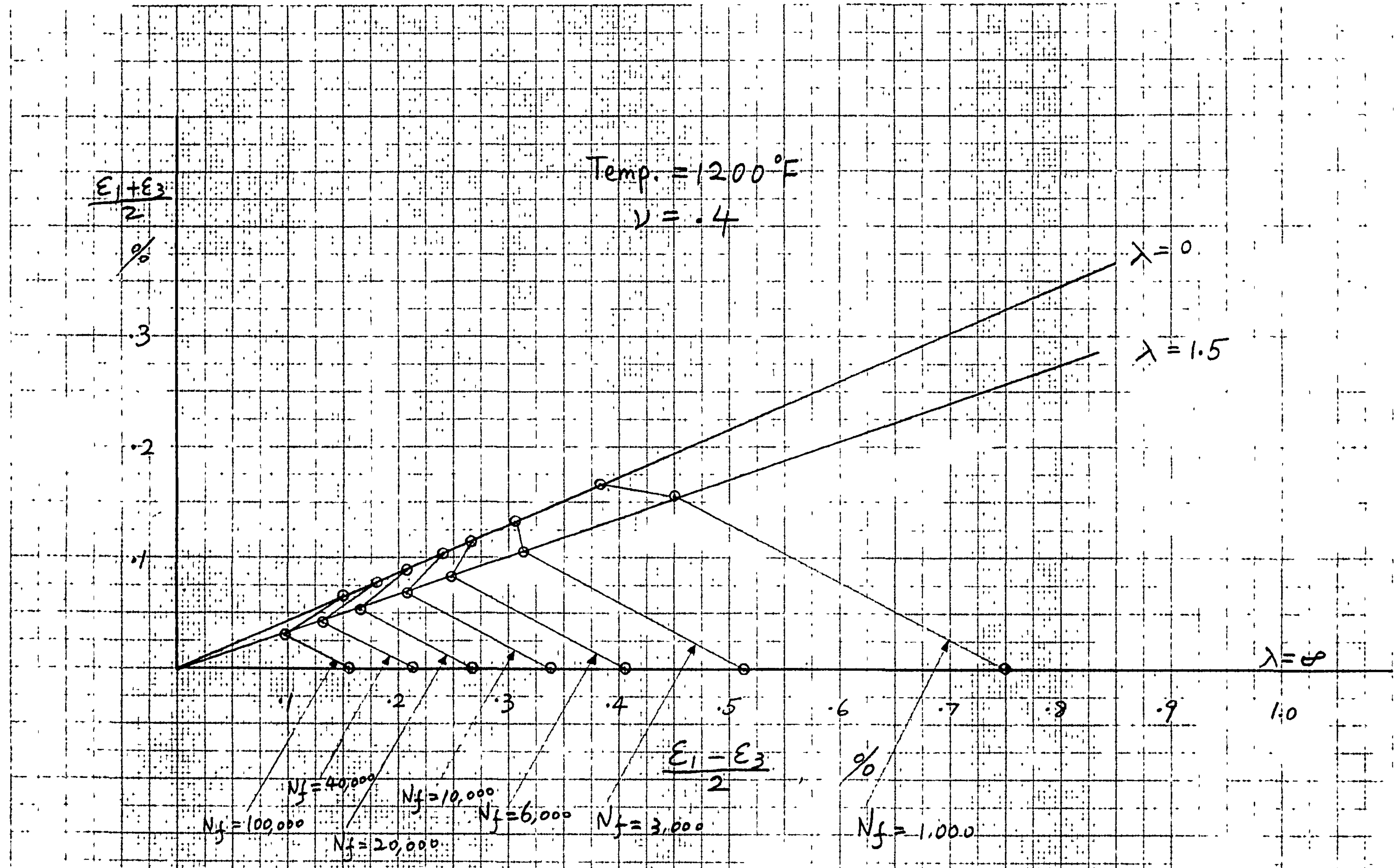

Temp. = 1200°F
$\nu = .4$
$\frac{\varepsilon_1+\varepsilon_3}{2}$ %
.3
.2
.1
$\lambda = 0$
$\lambda = 1.5$
$\lambda = \infty$
.1
.2
.3
.4
.5
.6
.7
.8
.9
1.0
$\frac{\varepsilon_1-\varepsilon_3}{2}$ %
$N_f = 100,000$
$N_f = 40,000$
$N_f = 20,000$
$N_f = 10,000$
$N_f = 6,000$
$N_f = 3,000$
$N_f = 1,000$

Fig. 12

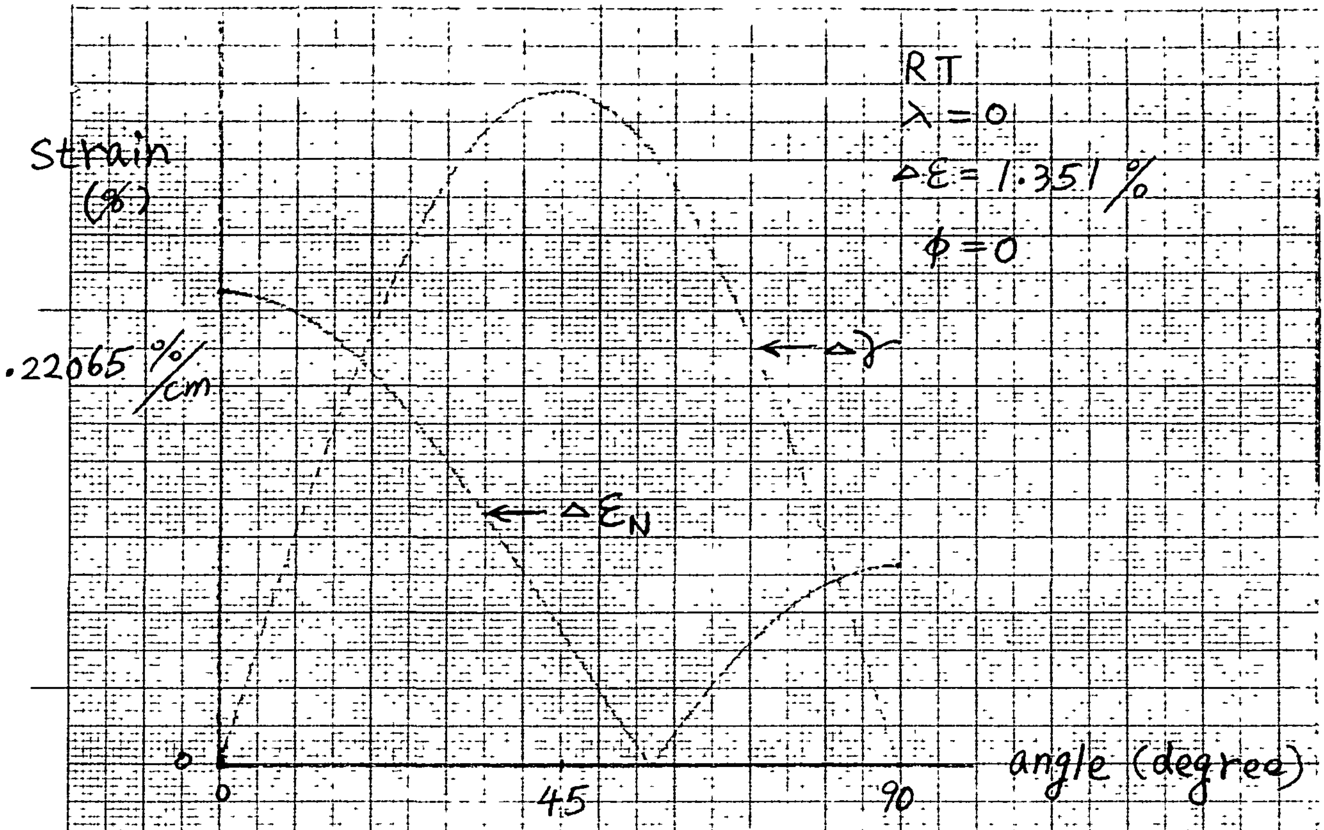
Strain (%)
.22065 %/cm
RT
$\lambda = 0$
$\Delta\varepsilon = 1.351\%$
$\phi = 0$
$\Delta\gamma$
$\Delta\varepsilon_N$
0
0
45
90
angle (degree)

Fig. 13

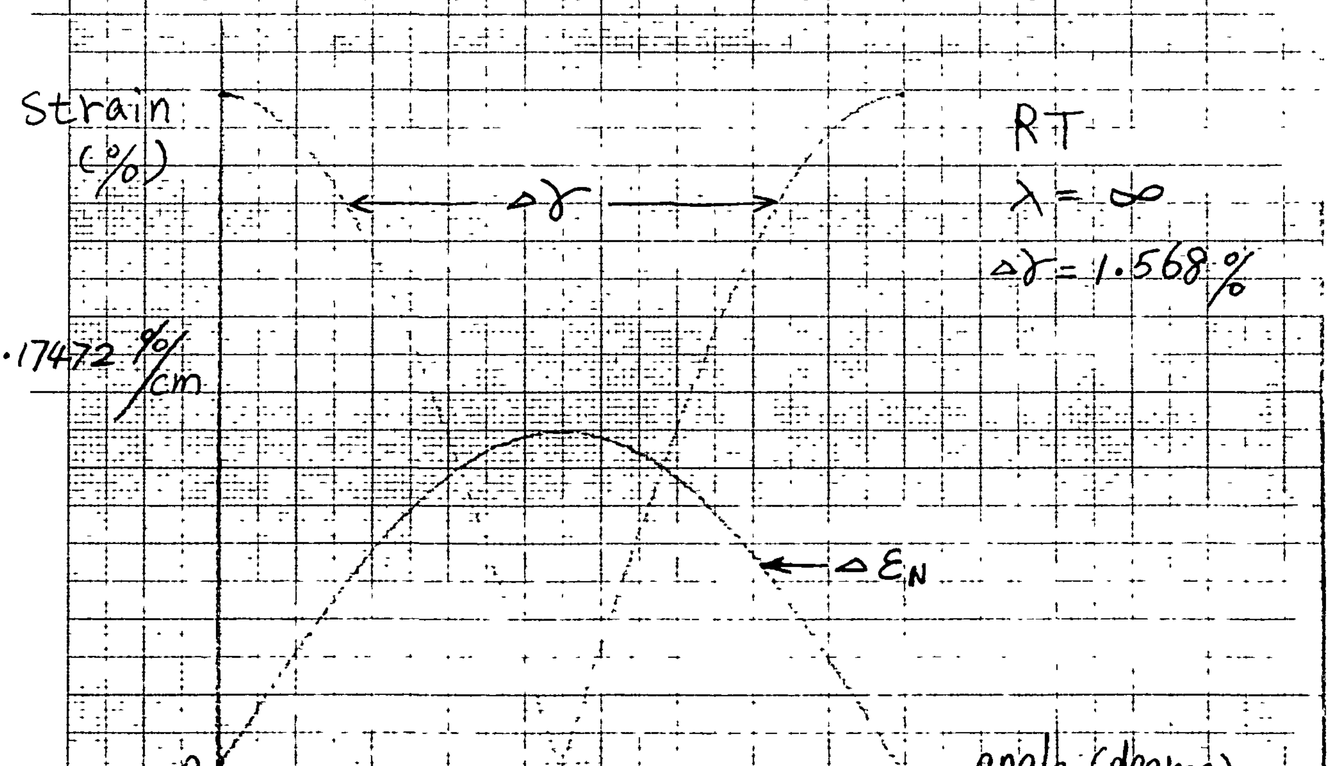
Strain (%)
RT
$\lambda = \infty$
$\Delta\gamma = 1.568\%$
$\Delta\gamma$
.17472 %/cm
$\Delta\varepsilon_N$
0
0
45
90
angle (degree)

Fig. 14

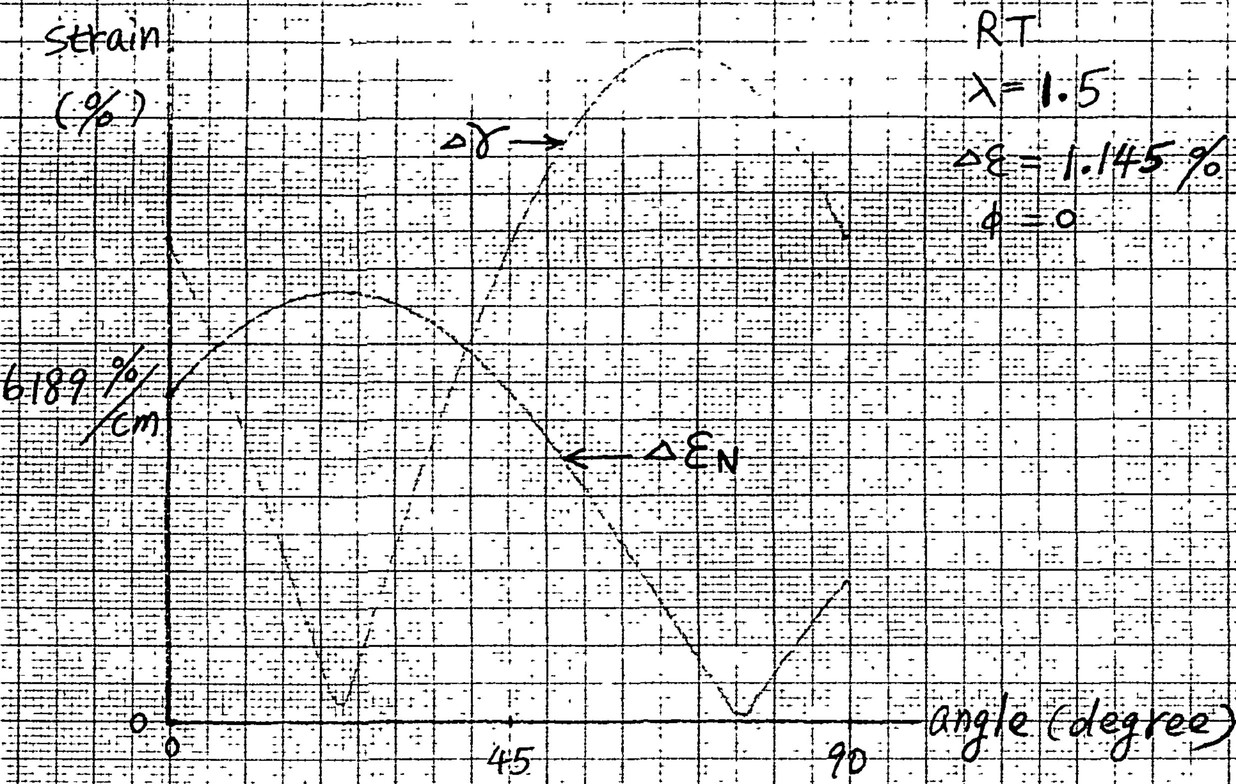
Strain
(%)
RT
λ = 1.5
Δε = 1.145 %
φ = 0
Δγ
.6189 %/cm
ΔεN
0
0
45
90
angle (degree)

Fig. 15.

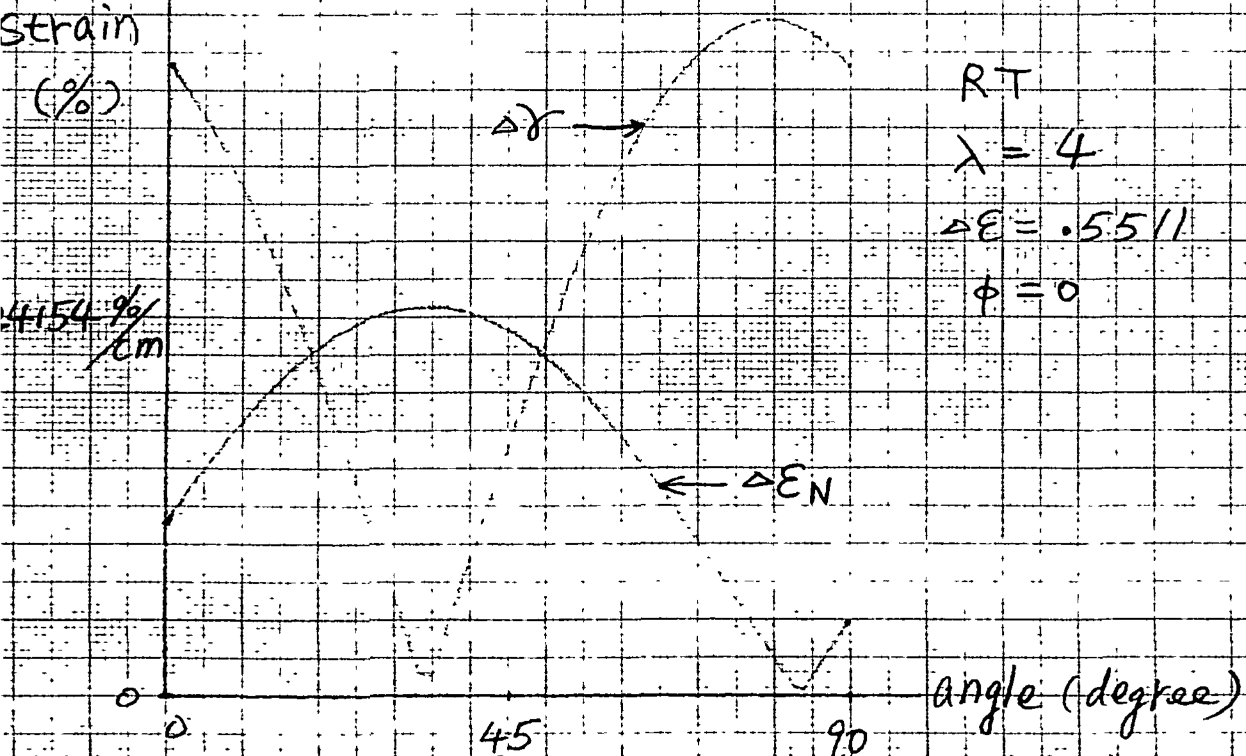
Strain
(%)
RT
λ = 4
Δε = .5511
φ = 0
Δγ
.4154 %/cm
ΔεN
0
0
45
90
angle (degree)

Fig. 16

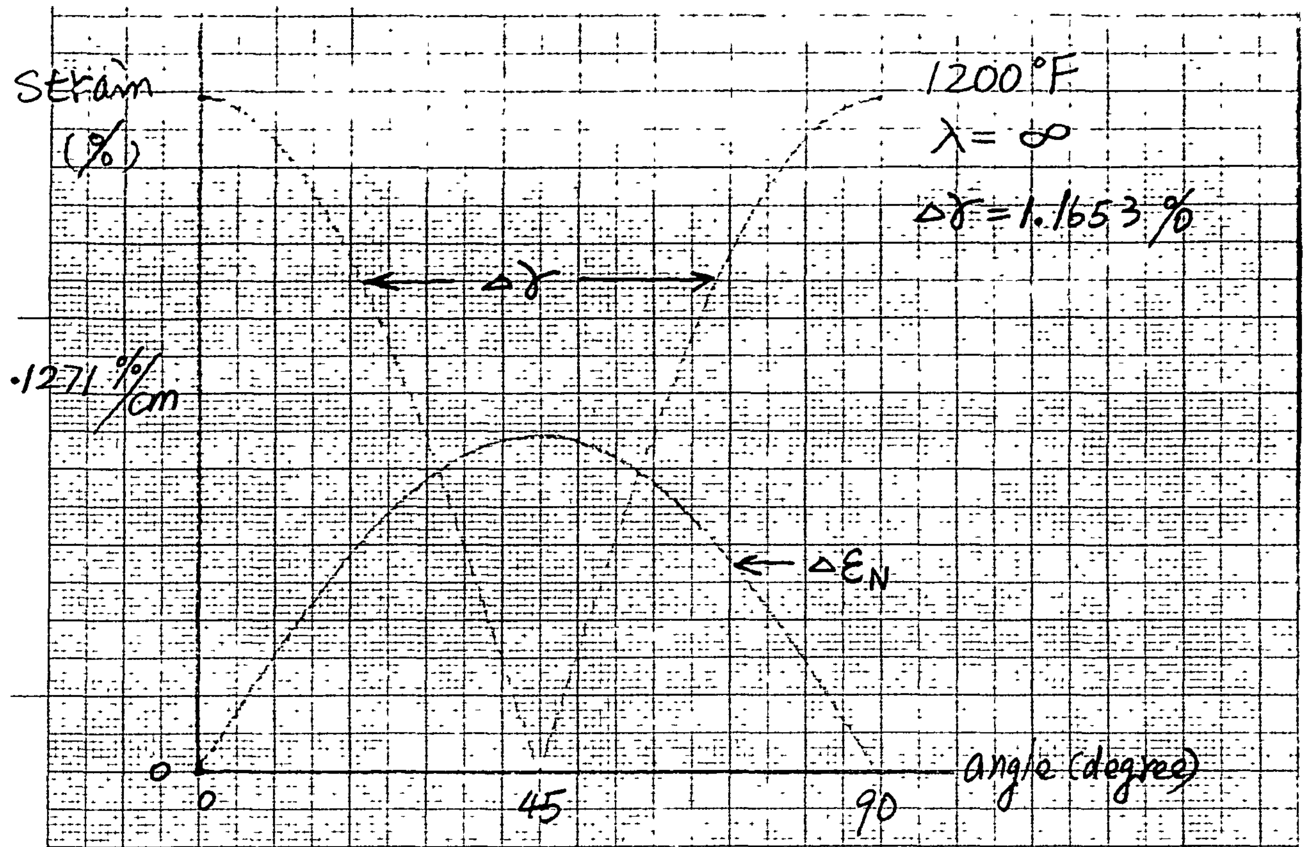
Strain
(%)
1200°F
λ = ∞
Δγ = 1.1653 %
Δγ
.1271 %/cm
ΔεN
0
0
45
90
angle (degree)

Fig. 17

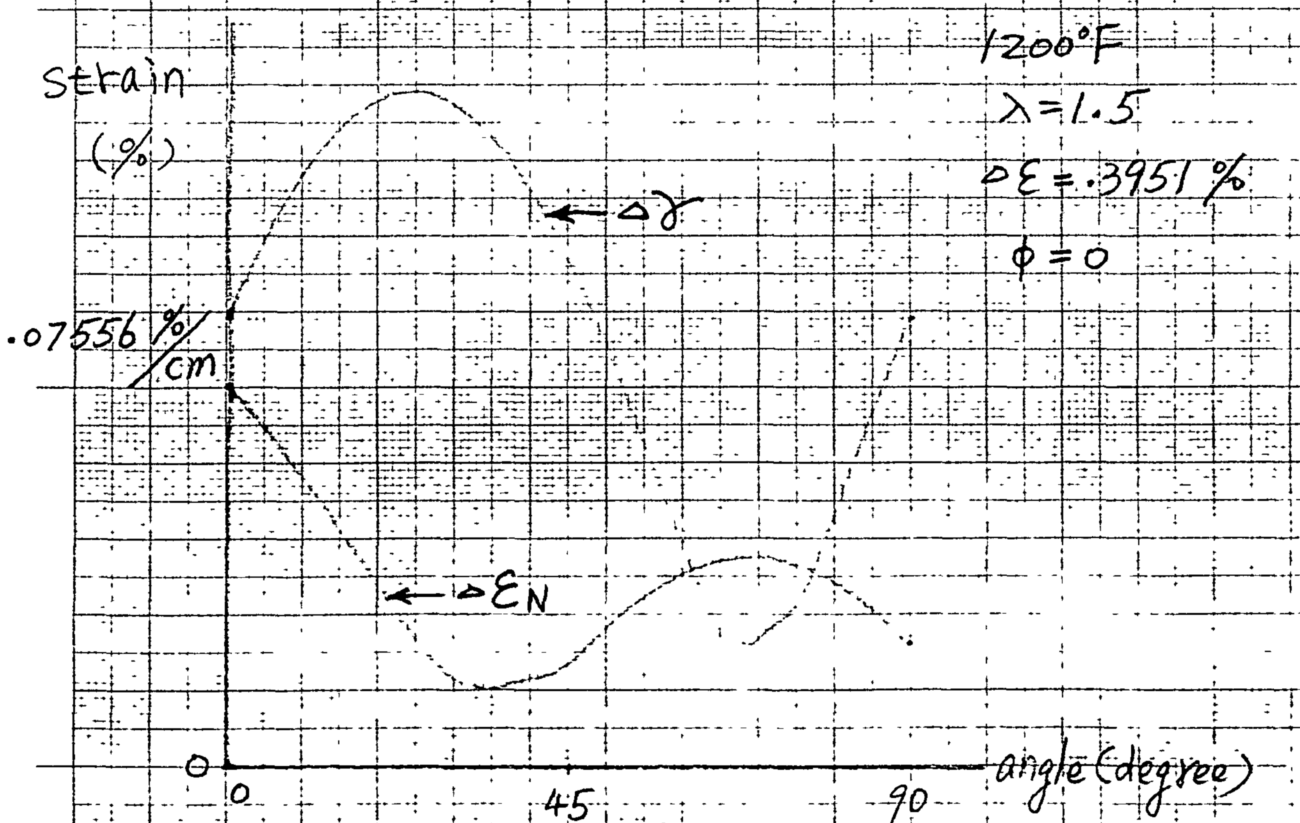
Strain
(%)
1200°F
λ = 1.5
Δε = .3951 %
φ = 0
Δγ
.07556 %/cm
ΔεN
0
0
45
90
angle (degree)

Fig. 18

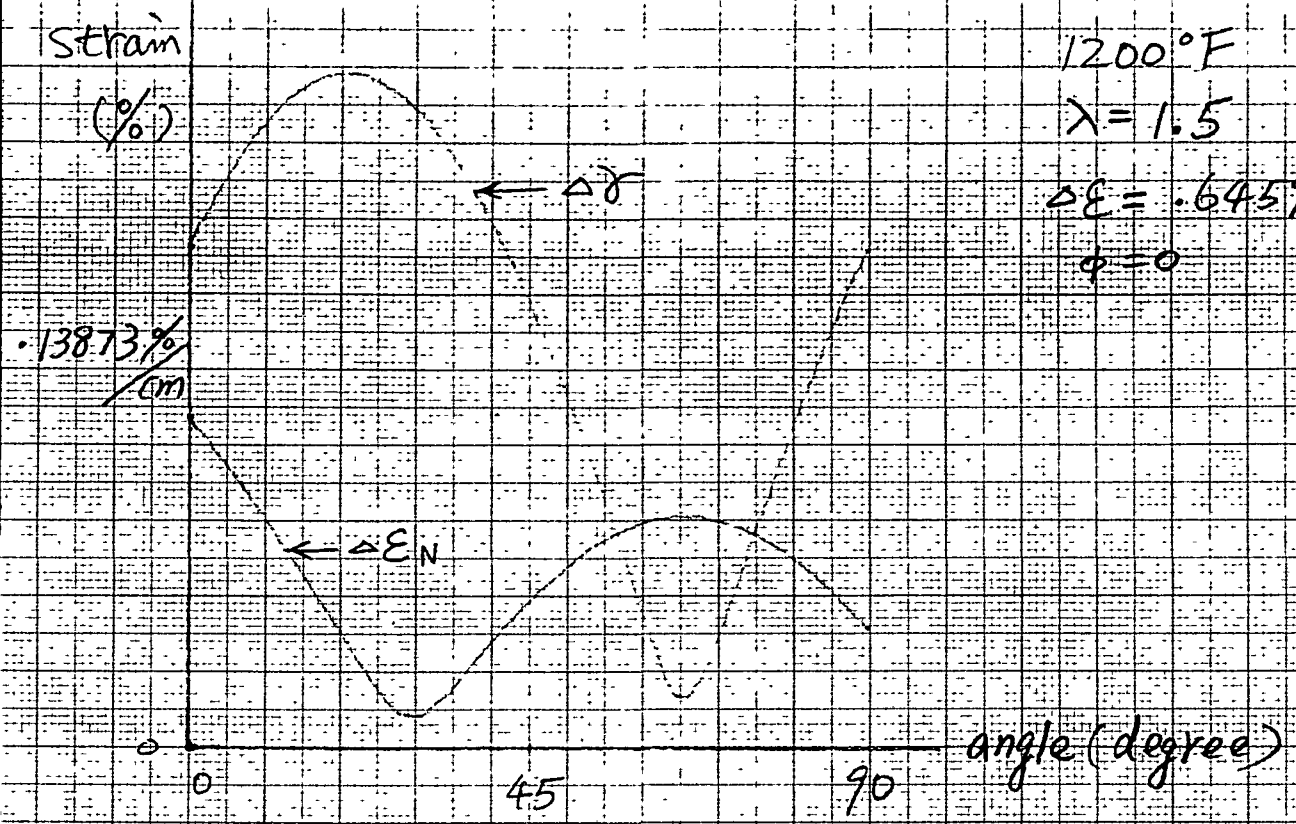
Strain
(%)
.13873%/cm
0
0
45
90
angle (degree)
Δγ
ΔεN
1200°F
λ = 1.5
Δε = .6459%
φ = 0

Fig. 19

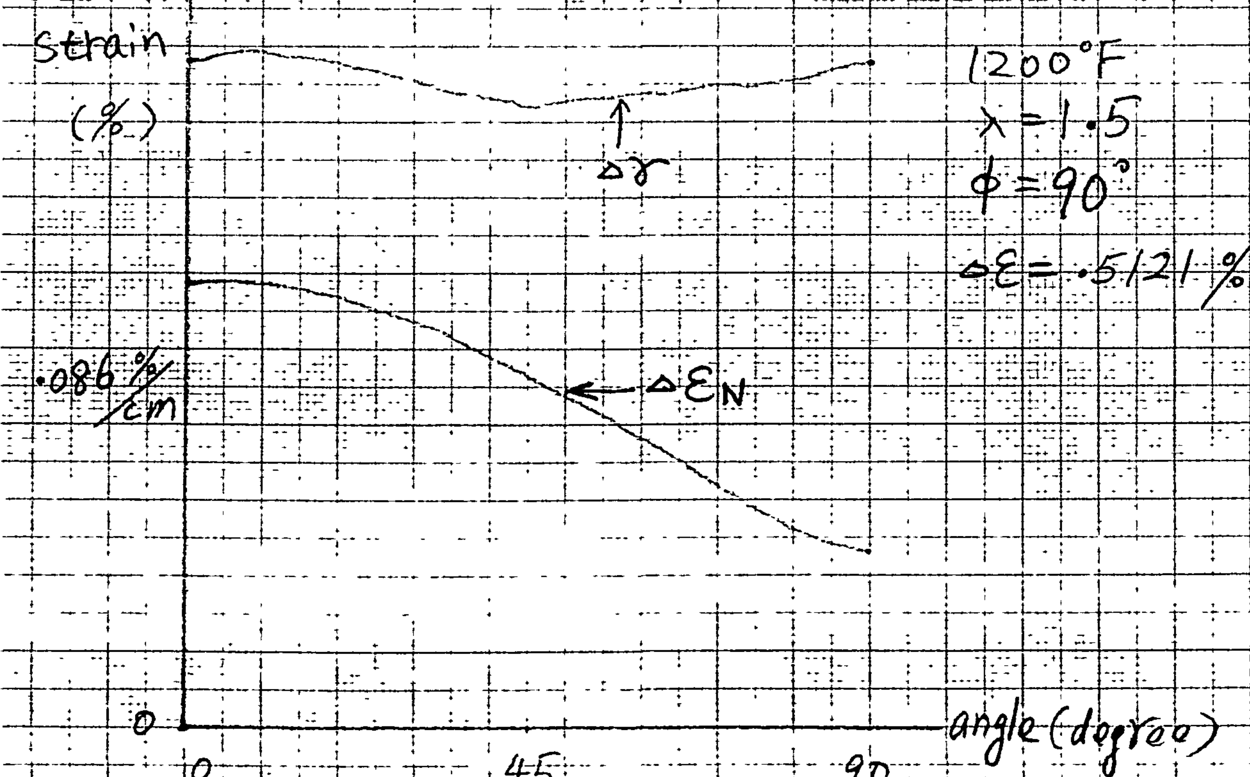
Strain
(%)
.086%/cm
0
0
45
90
angle (degree)
Δγ
ΔεN
1200°F
λ = 1.5
φ = 90°
Δε = .5121%

Fig. 20